The wave and plasma environments of Mars

Réjean Grard

Space Science Department of ESA, ESTEC, Keplerlaan 1, NL-2200 AG Noordwijk, The Netherlands

The principal characteristics of the wave and thermal plasma environments of Mars are reviewed, based on measurements performed with the electric field antenna and Langmuir probe carried by the Phobos 2 orbiter and on data collected with the radio occultation experiments and retarding potential analysers of the Viking orbiters and landers. The main regions and boundaries generated by the interaction between the planet and the solar wind are identified from the observed features; possible mechanisms for wave-particle phenomena are quoted, whenever possible. The foreshock region and bow shock of Mars present similarities with those of other planets, but the downstream subsonic transition region is markedly different from that seen at Venus. The nature of the obstacle remains ambiguous due to the absence of definite information about the possible existence of an intrinsic magnetic field.

THE harvest of information collected during the Phobos 2 mission has not only given us the long-needed knowledge about Mars and its interaction with the solar wind, but it has also triggered a re-examination of the data base accumulated during the Viking missions and has given a new momentum to comparative studies partly based on Pioneer Venus Orbiter measurements.

In spite of a relatively short lifetime around Mars (two months), a limitation in orbital coverage (only four periapsis crossings at an altitude of 850 km) and a deficiency of instrumentation (no magnetic search coil), the contribution of Phobos 2 to the present understanding of the martian environment remains primordial and, in several aspects, unprecedented.

The Phobos 2 wave and plasma data and relevant Viking measurements are reviewed in this article. The information is distributed in several chapters devoted to specific regions or boundaries, e.g. upstream region, bow shock, transition region and obstacle.

More information about the plasma and wave environments of Mars can be found in several issues of journals partly, or entirely, dedicated to this planet, e.g. *Nature* (Vol. 341, No. 6243, 1989), *Geophysical Research Letters* (Vol. 17, No. 6, 1990), *Planetary and Space Science* (Vol. 39, No. 1/2, 1991), *Journal of Geophysical Research* (Vol. 96, No. A7, 1991) and *Advances in Space Research* (Vol. 12, No. 9, 1992).

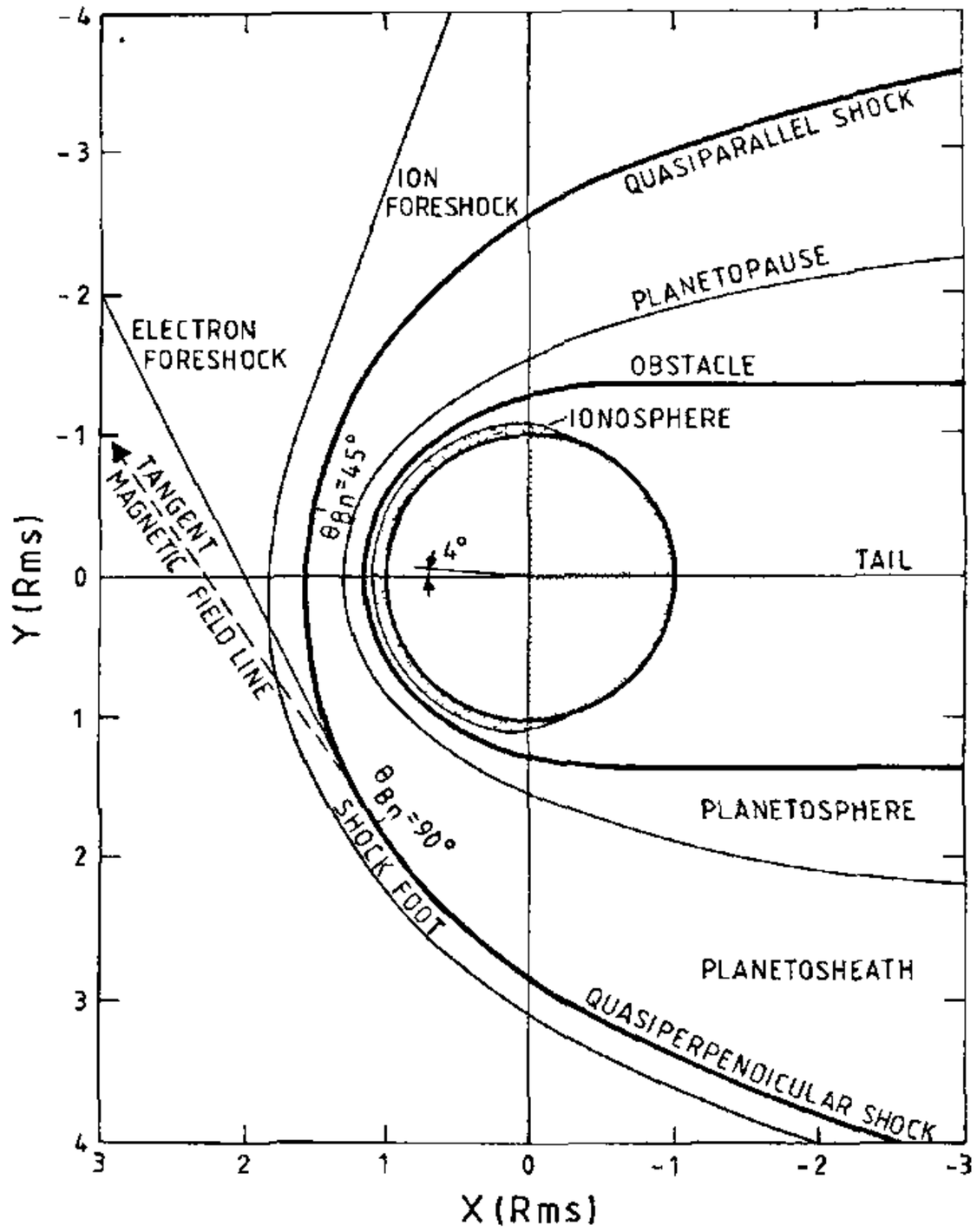

Figure 1. A schematic illustration of the martian plasma environment, approximately to scale

The model environment: morphology and terminology

Figure 1 describes the average configuration of the Martian environment and provides a frame of reference for the forthcoming discussion of plasma and wave phenomena.

Agreement on terminology is not unanimous and, in order to avoid possible misunderstandings, Figure 1 gives the names of regions and boundaries identified in the measurements or inferred from theory or simulation. The XY-plane is that of the martian ecliptic; the X-axis points towards the sun and the Y-axis lies along the dawn-dusk direction.

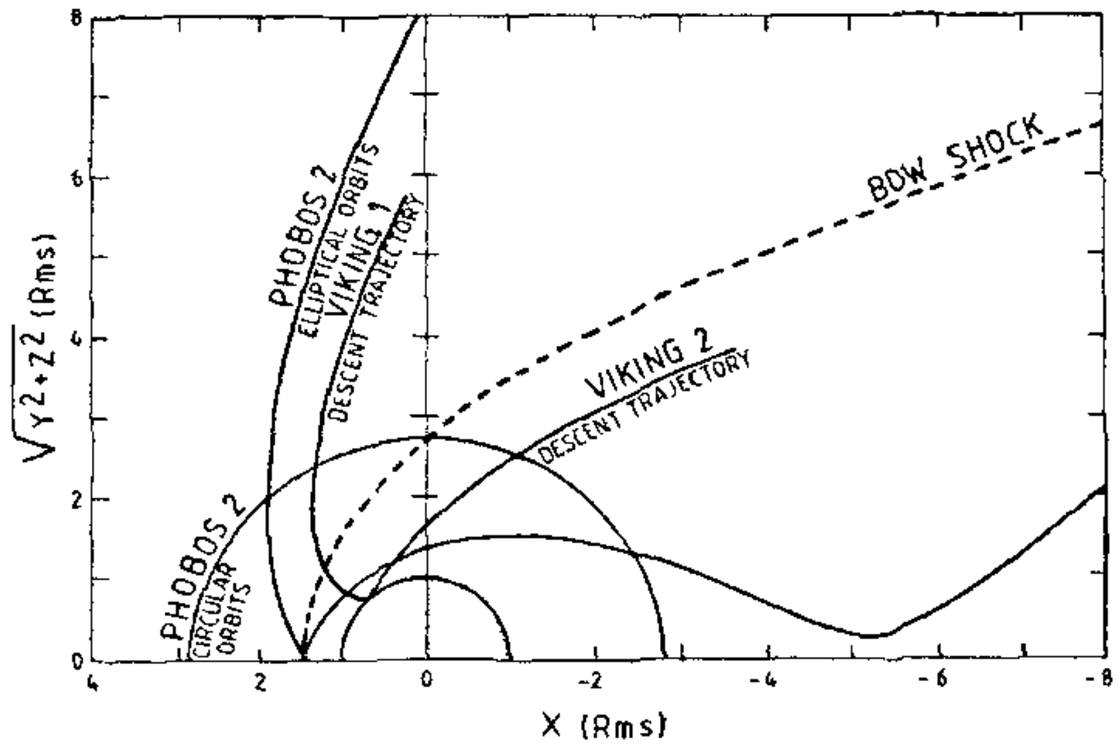

Figure 2. Descent trajectories of the Viking landers and typical orbits of Phobos 2. This spacecraft is moving in the equatorial plane of Mars which makes an angle of 20° with the XY-plane and rotates in the direct sense around the spin axis of the planet.

The ion gyroradius at Mars, about 1000 km for protons in the upstream region, is commensurate with the dimensions of the regions which compose the planetary plasma environment. This peculiarity entails a spatial asymmetry of the general morphology[1] and a lack of spatial definition of certain boundaries[2], as well as uncertainties about the tailward extent of regions which have only been clearly identified in the subsolar hemisphere.

The upstream region

The solar wind flow is antiparallel to the X-direction and the average spiral angle of the interplanetary magnetic field is 57°.

The electron foreshock is populated by particles which are accelerated at the shock and are backstreaming with energies of several 100 eV. Owing to the large velocity (relatively to the solar wind) and yet small gyroradii (a few km) of these suprathermal electrons, the associated boundary is practically tangent to the shock and makes an angle of only a few degrees with the field direction.

The ion foreshock and shock foot contain solar wind ions specularly reflected from the shock which are respectively convected away with the solar wind or returned to the shock after describing a partial gyration. The transition from foot to foreshock takes place at an angle between magnetic field and shock normal, θ_{Bn}, in the range 40-50°.

The bow shock

There is a general consensus on the nature and location of this boundary; the bow shock in the sunward hemisphere is represented by a surface of revolution having its symmetry axis tilted in the ecliptic plane by an angle of 4° with respect to the X-direction; this aberration is caused by the orbital motion of the planet in the radial flow of the solar wind. The average stand-off planetocentric distance of the bow shock is about 1.5 Rms at the subsolar point and 2.7 Rms at the terminator, corresponding to altitudes of 1700 km and 5800 km, respectively[3]. A tick marks the separation between regions where the shock is predominantly quasiparallel and quasiperpendicular ($\theta_{Bn} = 90°$).

The planetosheath

The region mostly populated by solar wind protons which lies between the bow shock and the planetopause is called planetosheath, but the word magnetosheath is met more frequently. The latter word is however ambiguous since it is also sometimes applied to the entire plasma volume convected with the solar wind magnetic field from the bow shock to the obstacle[4].

The planetopause

This boundary is observed at a mean planetary distance of 1.28 Rms, i.e. an altitude of 950 km for a solar zenith angle of the order of 55° (refs. 5, 6). The nature of the planetopause is still controversial, a situation reflected by the variety of names used for its identification.

Considered as a limit to the penetration of the solar wind protons but not to the penetration of the solar wind magnetic field, it is called planetopause, by analogy with Halley's cometopause[7,8] or magnetopause by analogy with the inner boundary of the Earth's magnetosheath[9-11]. This surface is also named ion composition boundary[6], because picked-up ions of planetary origin, mostly O^+, rather than protons are convected further downstream by the draped solar wind magnetic field.

The mass loading boundary, not shown in Figure 1, lies in the planetosheath, outside the planetopause, and should not be confused with the latter; it marks the outer limit of a transition region where the effect of planetary particles becomes noticeable[12]. The separation between these boundaries is only 100 km in the sunward hemisphere and is difficult to resolve but it reaches several 1000 km in the tail[6].

The planetosphere

The volume limited by the planetopause and the obstacle is called planetosphere[5]; the labels inner magnetosheath, O^+ mantle[4] and magnetosphere[13] are also used

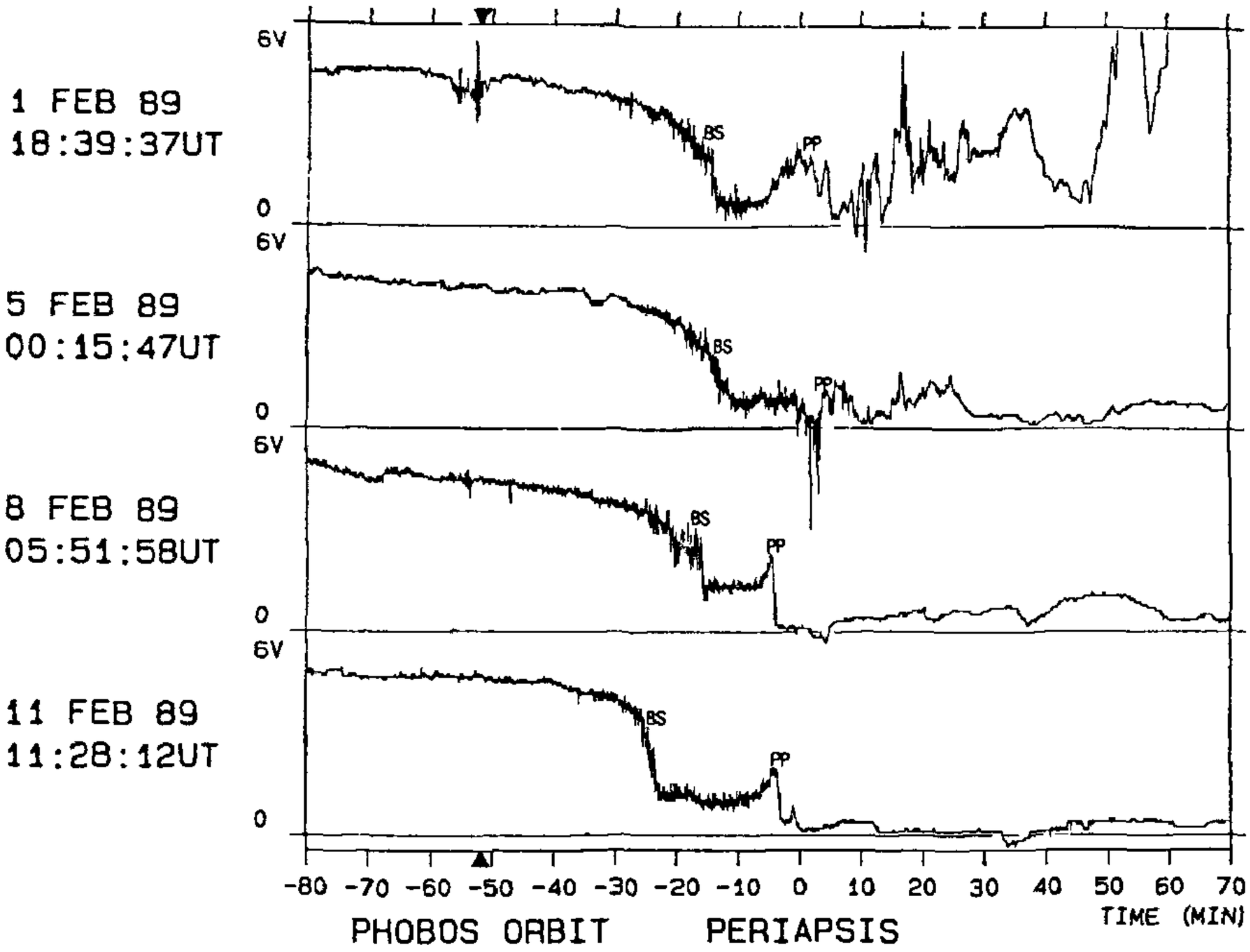

Figure 3. Floating potential of the Phobos 2 orbiter around the periapsis of the first four elliptical orbits The times of periapsis indicated on the left are taken as references The times at which the spacecraft is closest to the orbit of the Phobos moon, and crosses the planetary bow shock and planetopause, are marked by triangles, and the labels BS and PP, respectively

The obstacle

Gasdynamic modelling of the interaction between the solar wind and a planetary environment predicts that the martian bow shock observations call for an obstacle, distinct from the planetopause, at a height of the order of 500 km in the subsolar region[14]. This boundary which has never been unambiguously identified, experimentally, separates the possibly magnetized plasma practically at rest in the planetary frame from that which is convected by the solar wind magnetic field.

The surface of the obstacle is called magnetopause[15], or magnetic barrier, like at Venus[16], accordingly as the magnetization is caused by an inherent or induced field; it is also named ionopause[17, 18], irrespective or not of magnetization. The word magnetopause often applies to another boundary, namely the planetopause, and the locution magnetic barrier sometimes designates structures observed at larger planetary distances[13]. If confusions are to be avoided, the simple term obstacle[4] or force balance surface[6] should be preferred.

The nature of the obstacle is still debated. The existence of a dayside ionosphere is not questioned but its degree of magnetization by an induced or inherent field remains unknown. Other names have been proposed for the denomination of the obstacle: magnetosphere[14] and hybrid magnetosphere[15]. The extension of the obstacle which stretches out in the antisunward direction and is permeated by an induced magnetic field is called magnetotail[1, 19, 20] or planetotail.

Orbits and data base

Our knowledge about the bulk plasma density in the close martian environment is based on a series of radio occultation measurements performed with the American probes, Mariner 4, 6, 7 and 9, and orbiters, Viking 1 and 2, which have provided good spatial and temporal coverages of the ionospheric density distribution[21, 22]; two additional density and temperature profiles were acquired *in situ* with the retarding potential analysers of the Viking landers[23]. Plasma wave phenomena and

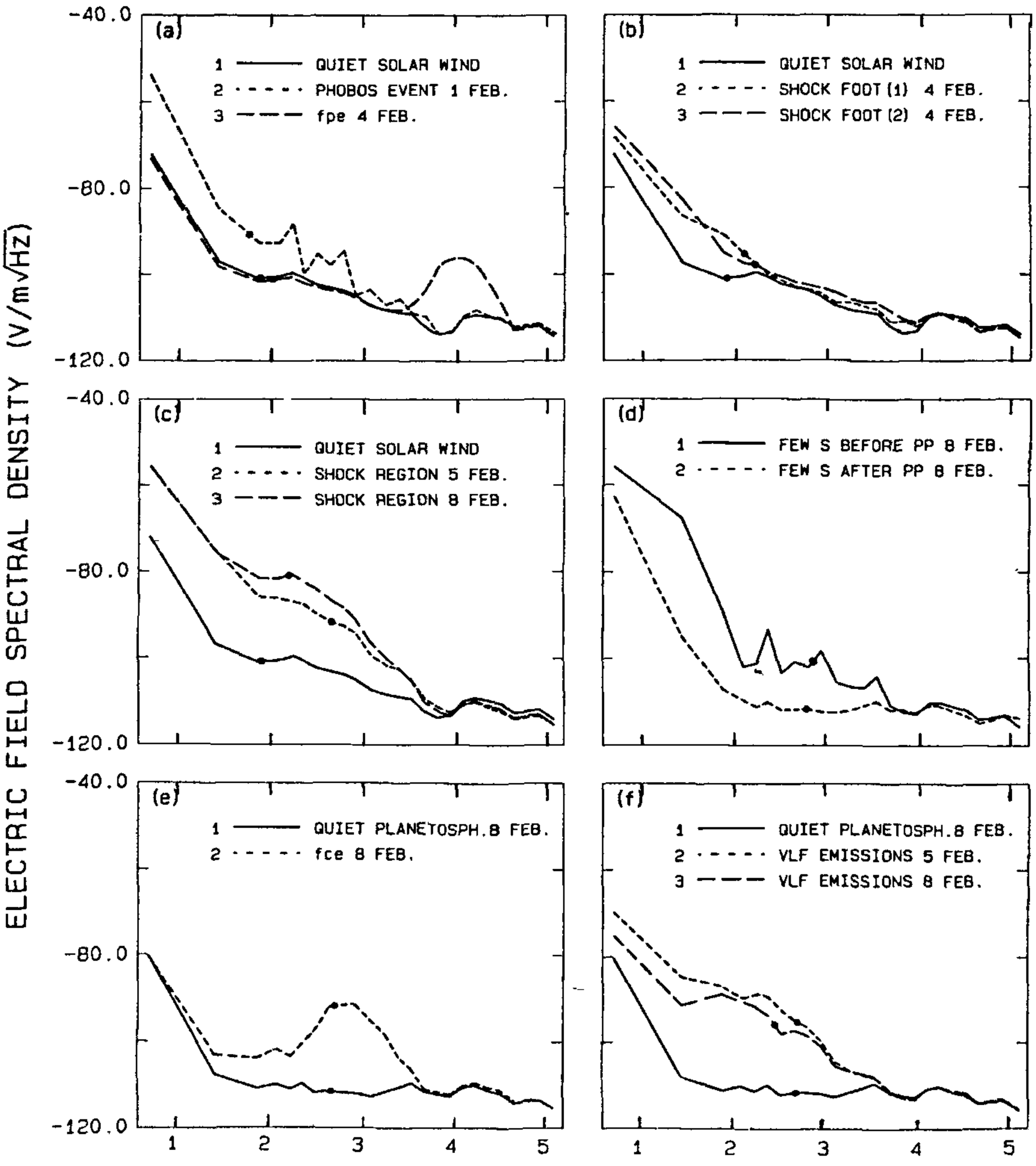

Figure 4. Typical electric field spectra Day of month (February), start time (UT) and averaging interval (s) of each spectrum are respectively: (*a*1, *b*1, *c*1) 4, 22 : 30 : 07, 120, (*a*2) 1, 17 : 47 : 09, 10, (*a*3) 4, 23 : 27 49, 40, (*b*2) 4, 23 · 47 : 13, 120, (*b*3) 4, 23 : 52 : 37, 120; (*c*2) 5, 00 : 02 : 07, 120, (*c*3) 8, 05 : 31 : 01, 120; (*d*1) 8, 05 : 48 · 05, 2, (*d*2) 8, 05 : 48 : 33, 2, (*e*1, *f*1) 8, 06 : 02 : 49, 120, (*e*2) 8, 05. 55:37, 2; (*f*2) 5, 00·31 01, 90; (*f*3) 8, 06 10 43, 120 A dot marks the average electron gyrofrequency associated with each spectrum.

electron density and temperature were observed in the more distant environment of Mars with the electric antenna and Langmuir probe carried[24] by the Soviet orbiter, Phobos 2; no wave magnetic field measurements are available at frequencies larger than 10 Hz.

The Viking 1 and 2 landers reached the surface of Mars at solar zenith angles of about 44°, on 20 July and 3 September 1976. Phobos 2 described 4 elliptical orbits in the equatorial plane of the planet during the period 29 January–12 February 1989, with periapsis at typical altitude and solar zenith angle of 854 km and 51°; the orbiter was subsequently transferred to a circular orbit very close to that of the Phobos moon at an average altitude of 6200 km, where it was operated[25] until March 1989.

The descent trajectories of the Viking landers and the orbits of Phobos 2 are plotted in cylindrical projection, in Figure 2; the X-axis is pointing towards the sun and the average location of the non-aberrated bow shock is shown as a line of reference. This figure illustrates only too well the present paucity in spatial coverage of *in situ* plasma and wave measurements.

Upstream region

Phobos torus

The interaction between the torus of the martian moon, Phobos, and its environment does not strictly belong to the class of planetary phenomena covered in this review; it is nevertheless briefly described for completeness. The crossing of the gas/dust torus which encapsulates totally, or partially, the orbit of the Phobos moon is most easily identified upstream of the martian bow shock and of the ion and electron foreshocks, where no other interaction is usually visible.

Approximately 50 minutes before periapsis, spacecraft potential measurements* reveal, clearly on the first orbit and, to a lesser extent, on the third one, an electron flux increase associated with photoemission, secondary emission or ionization of molecules sputtered from a dust torus generated by the moon (Figure 3). At the time of the 1 February event, the spacecraft was at a distance of 4000 km from the moon and 400 km from its orbit[26]. The frequency spectrum of the electric field is shown in Figure 4 *a* (curve 2); it reveals, with reference to the quiet solar wind (curve a1), an enhancement of the wave activity in a range which extends beyond the local electron gyrofrequency. This activity reflects the interaction of the solar wind with a mixture of ions, electrons and positivity charged grains with dimensions[27] larger than 1 μm.

These observations are corroborated by independent charged particle and magnetic field measurements performed, not only in the solar wind, but also within the bow shock, in the vicinity of the two martian moons, Phobos and Deimos[26, 28]. Any confusion between the torus effect seen in Figure 3 and a foreshock event[29] is therefore most unlikely.

Disturbances are also observed in the tails of these two moons and are reminiscent of an interaction between the solar wind and a comet[30, 31].

Electron foreshock

Electron plasma oscillations are generated by electron beams which are accelerated at the bow shock and travel upstream in the solar wind along a direction practically parallel to the magnetic field; this instability develops therefore on field lines which are connected to the shock, near the boundary of the electron foreshock (Figure 1). These emissions are visible in the top panel of Figure 5 in a frequency range nearly centred on the local electron plasma frequency, $f_{pe} \simeq 13$ kHz, which corresponds to a plasma density of about 2 cm^{-3}. The average spectral distribution in a time interval of 40 s starting at 23:27:49 UT is also shown in Figure 4 *a* (curve 3).

Due to the predominant orientation of the upstream magnetic field and on account of the particular configuration of the Phobos 2 circular orbit (Figures 1 and 2), it can be verified in Figure 6 that the instability is, on average, seen more often in the morning sector. These electrostatic waves have amplitudes of a few mV/m and are polarized along the direction of the local magnetic field[32]. They are similar to those previously observed in the foreshocks of other planets, for example Earth[33] and Venus[34].

Shock foot and ion foreshock

The outer edge of the shock foot or ion foreshock is crossed three times on 4 February (Figure 5, panel 2). Differentiation between the shock foot and the ion foreshock is not always possible on this type of orbit because θ_{Bn} does not differ markedly from 45° at the subsolar shock (Figures 1 and 2).

The foot has a thickness of the order of one ion gyroradius ($\simeq$1000 km) and is populated by solar wind protons which are specularly reflected from a quasi-perpendicular shock[2]. The ion foreshock, on the contrary, develops in the vicinity of a quasiparallel shock; it contains particles which diffuse from this boundary and are convected away by the solar wind.

*The floating potential of a spacecraft is measured with respect to a reference electrode. This potential is anticorrelated with the ambient electron flux, positive in a rarefied medium (e.g. 5 V in the solar wind), it may reach negative values in dense and/or energetic environments. The plasma density can be deduced from the floating potential if the electron temperature is known[13].

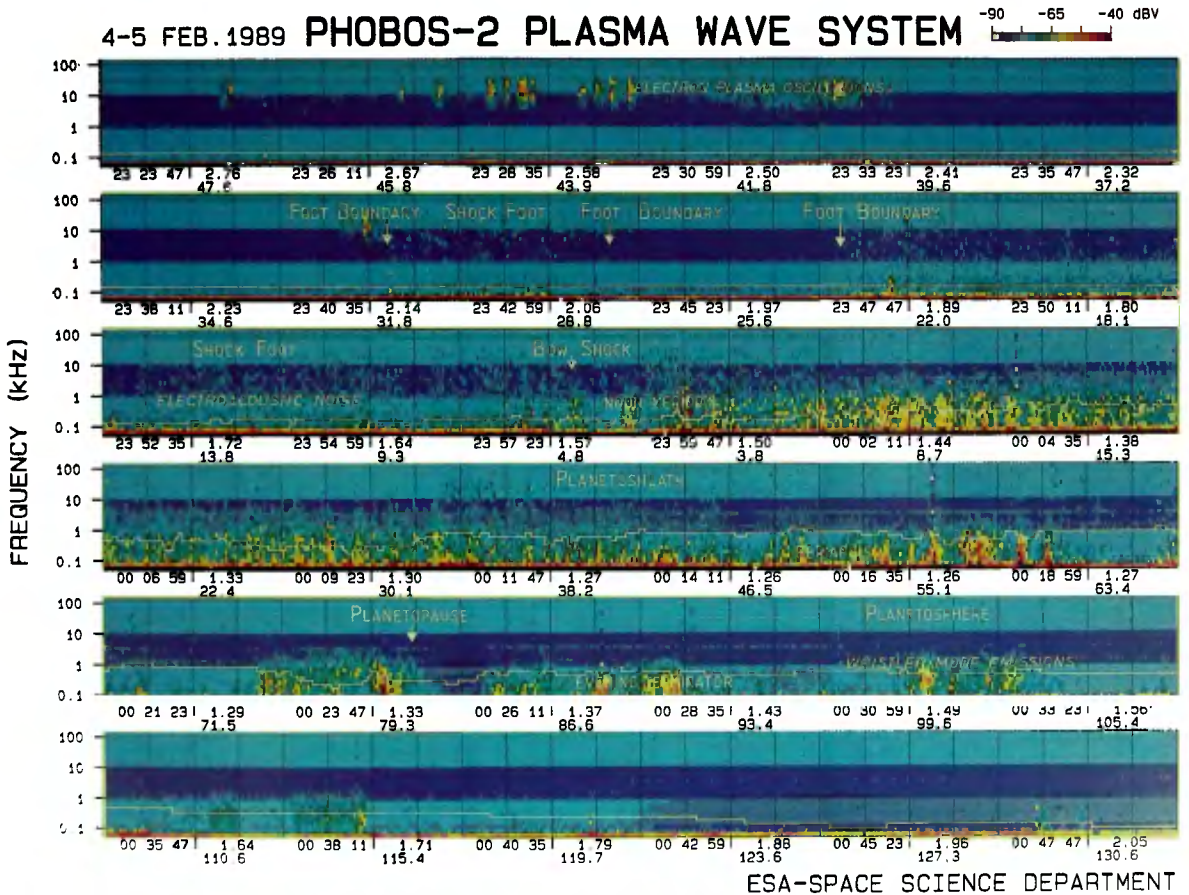

Figure 5. Dynamic spectrogram of the electric signal recorded by Phobos 2 on the second elliptical orbit This raster represents the information delivered by 25 contiguous filters The level is given by the colour scale shown at the top right the effective length of the antenna is 1 45 m and –40 dB corresponds to 10 mV U1, areocentric distance (Rms) and below solar zenith angle (degrees) are given along the horizontal axis The white line gives the electron gyrofrequency

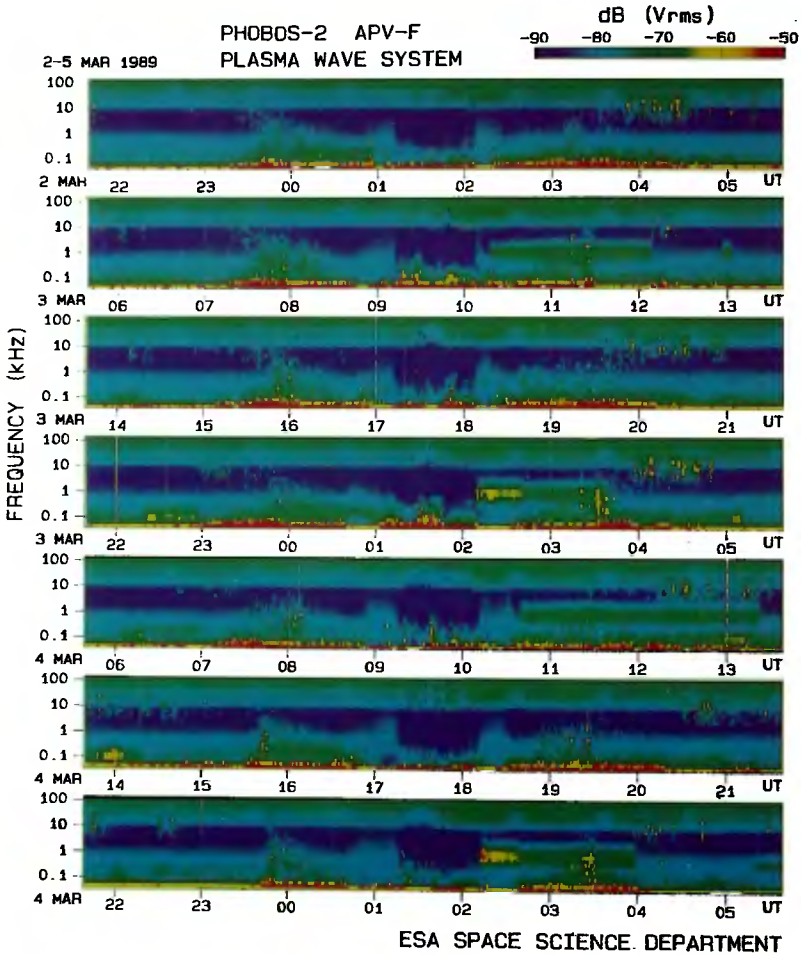

Figure 6. Dynamic spectrograms recorded during 7 successive circular orbits centred around local midnight. The bow shock is crossed in the vicinity of the evening (morning) terminator approximately 2 hours before (after) local midnight. The steady signal visible around 1 kHz in the morning sector of orbits 2, 4, 5 and 7 is an on-board interference. See Figure 5 for additional information.

The spectrum of the noise is illustrated by curves 2 and 3 of Figure 4*b*. This wave is associated with a Doppler shifted ion acoustic instability in the foreshock[35] and a lower hybrid oscillation in the foot[36].

The level and turbulence of the electron flux (anticorrelated with the spacecraft potential) increase progressively during the traversal of this region, corresponding to a time interval of about 20 minutes before the bow shock crossing (Figure 3). This trend is also visible in the electron density, independently measured with a Langmuir probe, which is displayed in the second panel of Figure 7.

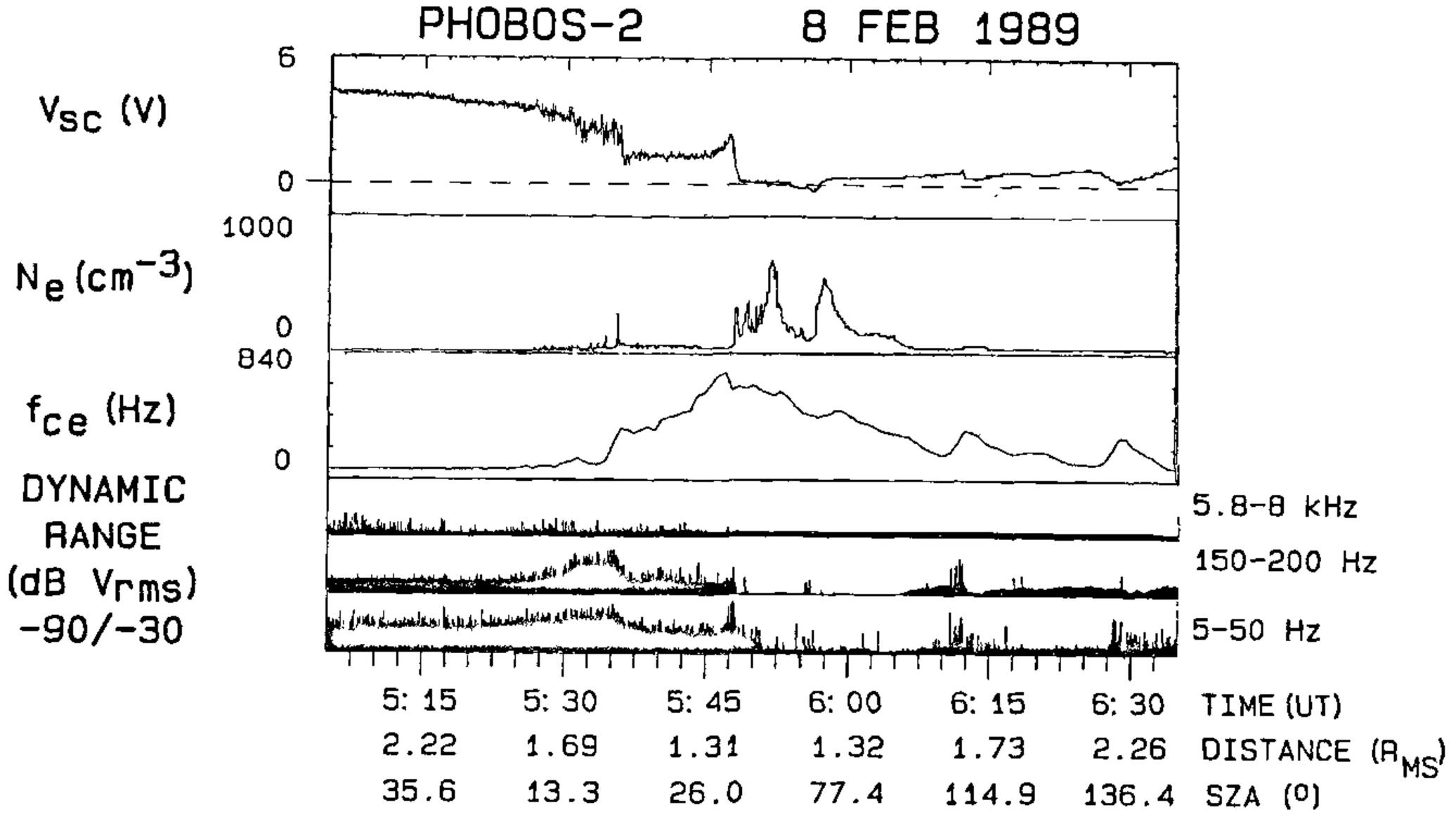

Figure 7. Plots of the spacecraft potential V_{sc}, electron density N_e, electron gyrofrequency f_{ce} and electric field levels in three frequency ranges, against universal time, areocentric distance and solar zenith angle around the periapsis of the third elliptical orbit of Phobos 2. The bow shock and planetopause crossings are observed at 05:36 and 05.48, respectively.

Magnetohydrodynamic turbulences are also observed with the magnetometer at the proton gyrofrequency, with a left-hand polarization[29]; they are associated with diffuse ions in the foreshock and pick-up protons elsewhere (Figure 8).

Bow shock

The bow shock is easily identified as a marked increase of the ambient electron flux due to a rapid deceleration and energization of the solar wind plasma (Figure 3). An average model configuration of the bow shock has been derived from these observations[37], in good agreement with models inferred from magnetic field measurements[3].

The evolution of the wave spectrum is not as spectacular (Figure 5, panel 3) and varies from orbit to orbit (Figure 9). The four recordings shown in Figure 9 represent all the wave data presently available in the close vicinity of the subsolar shock. The angle θ_{Bn} is 41° for the first crossing, 45–60° for the second one and 45° for the third one[38], values not too different from that of the model configuration, 57° (Figure 1). No d.c. magnetic field data are available for the fourth orbit.

In spite of seemingly similar conditions, the onset of the broadband noise does not always occur at the same distance from the shock, The activity enhancement, most visible on the third orbit, is probably due to the sporadic role of ionospheric ions or atmospheric neutrals which are ionized in the solar wind by the critical ionization velocity phenomenon or other processes. Such an interpretation is supported by the fact that the martian shock spectrum most resembles the spectrum recorded during the AMPTE lithium release, which may indicate the presence of pick-up ions[39].

Figure 6 displays for comparison a continuous dynamic spectrogram recorded during 7 successive circular orbits with a period of exactly 8 hours; note that the colour scales of Figures 6 and 9 are identical. The bow shock is crossed at around 23:30 and 03:30 UT (± 8 hours); the wave activity appears to be much less intense at the terminator (altitude 1.7 Rms) than in the subsolar area (altitude 0.5 Rms) due, in part, to the reduction of escaping planetary plasma density with increasing distance.

Two examples of bow shock spectra are given in Figure 4*c*; spectrum 2 is taken in the overshoot and spectrum 3 in the ramp, i.e. immediately after and before the shock[40,41]. Figure 10 compares the spectra recorded in the shock regions of Earth and Mars with Phobos 1 and Phobos 2, in the same format as those reported by Scarf *et al.*[42] and Gurnett[35] for Venus, Jupiter and Saturn. The signals measured with Phobos 1, Phobos 2 and Pioneer appear to be artificially enhanced above 10 kHz, due to the relatively low signal-to-noise

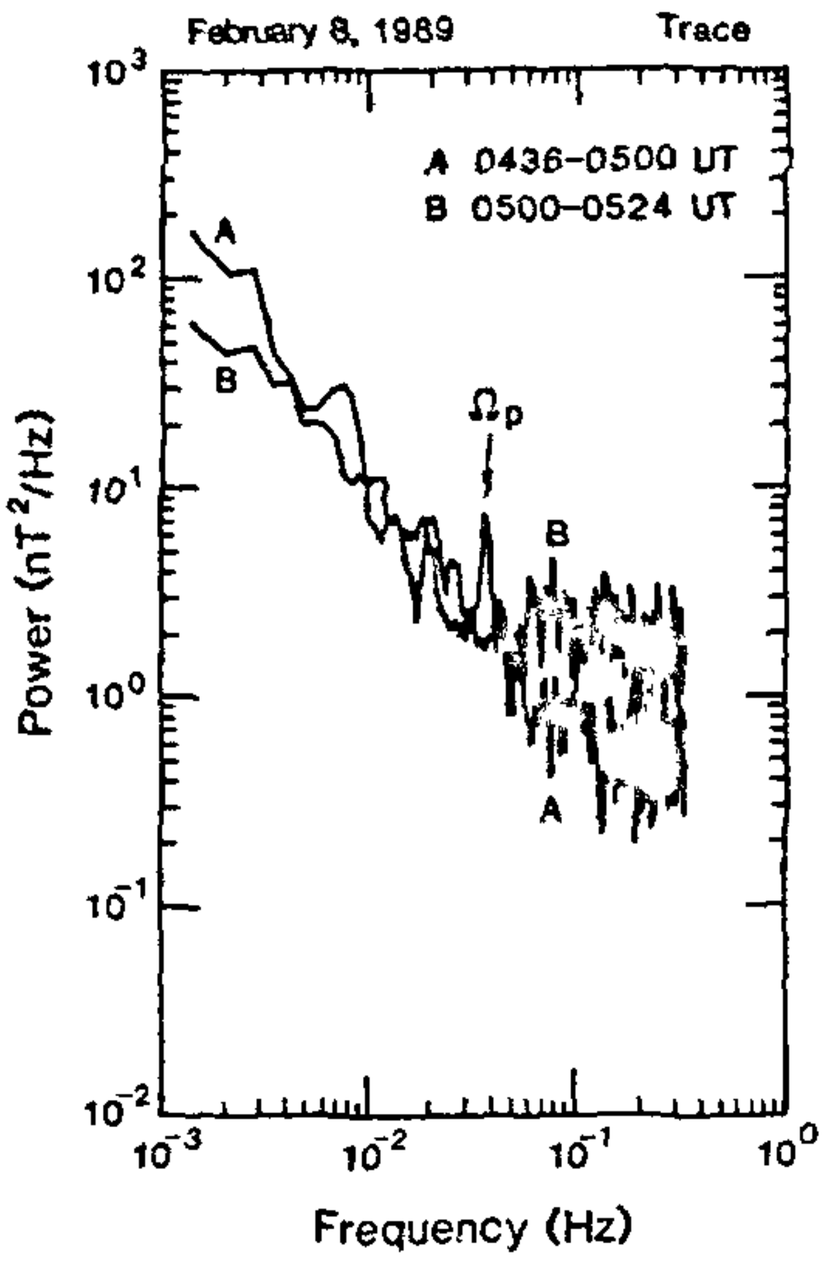

Figure 8. Power spectra (A) before and (B) during the detection of a tone at the proton gyrofrequency upstream of the bow shock on 8 February 1989 (ref 29)

ratios which can be achieved with short electric antennas.

The shapes of the spectra are similar and scaled by the characteristic frequencies of the solar wind plasma: electron gyrofrequency (f_{ce}), ion and electron plasma frequencies (f_{pi}, f_{pe}), Buneman mode characteristic frequency ($f_B = [m_e/m_i]^{1/3} f_{pe}$, where m_e/m_i is the electron–ion mass ratio) and Doppler shift frequency for ion acoustic waves ($V_{SW}/2\pi\lambda_D$, where V_{SW} is the solar wind velocity and λ_D the Debye length). The spectra result from the superposition of electromagnetic waves with frequencies less than f_{ce} (whistler mode) and ion acoustic instabilities with wavelengths of the order of λ_D and frequencies shifted by V_{SW}/λ_D in the frame of reference of the satellites[35].

Transition region

The transition region extends from the bow shock to the obstacle and contains the downstream subsonic flow of a plasma consisting mostly of solar wind protons in the planetosheath and planetary ions (O^+) in the planetosphere.

The deceleration of the solar wind is caused by ion pickup and charge exchange in the planetosheath and, mostly, by momentum transfer through the planetopause to planetary ions which escape from the ionosphere and enter the planetosphere[43].

Planetosheath

One of the main features of the planetosheath, which, according to our definition, is the region which lies between the shock and the planetopause (*Figure 1*), is the continuation of the turbulences which characterize not only the plasma electron flux and density (Figures 3 and 7) but also the ambient magnetic field[44]. One observes also a progressive decrease of the Doppler shifted acoustic waves with frequencies above f_{ce} (*Figure 5, panels 3–5*).

Planetopause

The wave and plasma properties are so drastically different on both sides of the planetopause that this boundary is sometimes deliberately confused with the obstacle, rather than recognized as the inner boundary of a transition region where solar wind protons have been progressively replaced by planetary ions.

The planetopause is not believed to play the role of an obstacle because its location is too high in altitude and does not appear to be much influenced by the variations of the solar wind pressure[6].

The standing feature which discloses the inbound crossing of the planetopause is the disappearance of the rapid magnetic field and electron flux turbulences (Figure 3). This boundary cannot otherwise be always recognized, unambiguously, from wave measurements alone (Figure 5, panel 5). The third inbound crossing of Phobos 2 is a particularly clear example which exhibits most simultaneous features (Figure 7); the electron density profile shows a marked discontinuity because the plasma diffusing from the planetosphere is constantly removed from the planetosheath where the solar wind convection is more efficient[6], the very sharp decrease of the wave activity is illustrated by the lower panel of Figure 7 and the two spectra of Figure 4*d* which compares the wave energy distribution upstream (spectrum 1) and downstream (spectrum 2) of the planetopause. The surge of wave activity which is seen in the 5–50 Hz frequency range at exactly the time of the planetopause crossing (Figure 7, bottom panel) is probably an electrostatic wave close to the lower hybrid frequency resulting from an interaction between the two ion populations which prevail on both sides of the boundary, as observed outside the ionopause of Venus[45].

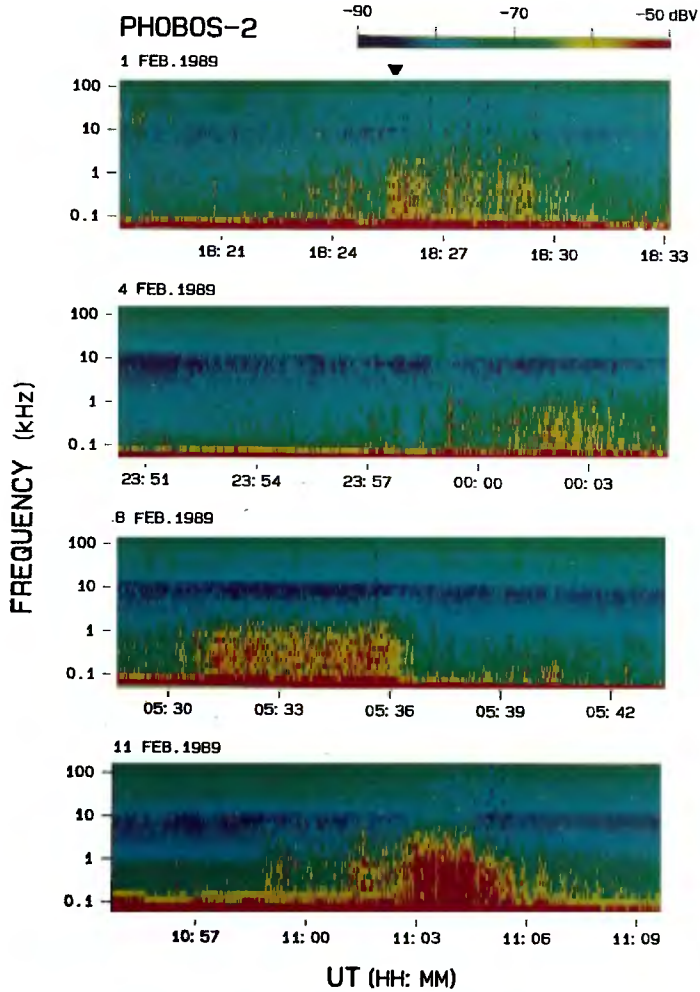

Figure 9. Dynamic spectrograms recorded during time intervals of 15 minutes centred around four inbound shock crossings which are aligned with the triangle shown at the top centre of the first panel. See Figure 5 for additional information

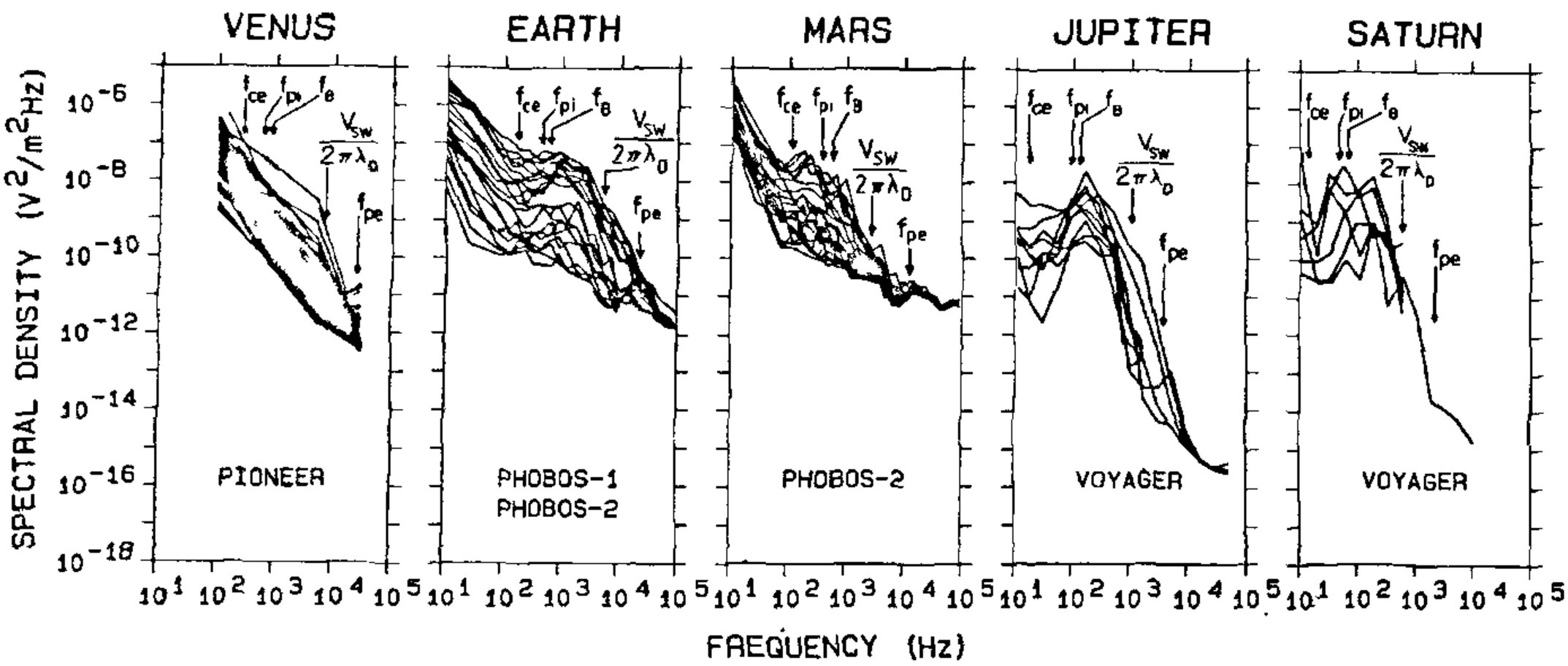

Figure 10. Comparison between the electric field spectral densities observed at the bow shocks of five planets. The Venus, Jupiter and Saturn data are taken from Scarf *et al*[42] and Gurnett[35]. The Earth measurements were performed with Phobos 1 and Phobos 2 on 2 and 13 July 1988, a few hours after the launches. The Mars measurements were collected with Phobos 2 on 4 and 8 February 1989.

Planetosphere

The planetosphere is an extremely complex and fluctuating environment; its structure is partly controlled by the planetary ion population and presents very different profiles from one orbit to the next (Figure 3). Plasma clouds with densities of up to 700 cm^{-3} and electron mean kinetic energies of the order of 1 eV develop a dynamic pressure equivalent to that of a 20 nT magnetic field and play a significant role in convection processes. Anticorrelated fluctuations of magnetic field and electron density recorded at distances of 8–10 Rms, in the tail planetosphere, are shown in Figure 11. Figures 4 *e* and *f* illustrate the variety of wave phenomena also observed in this region.

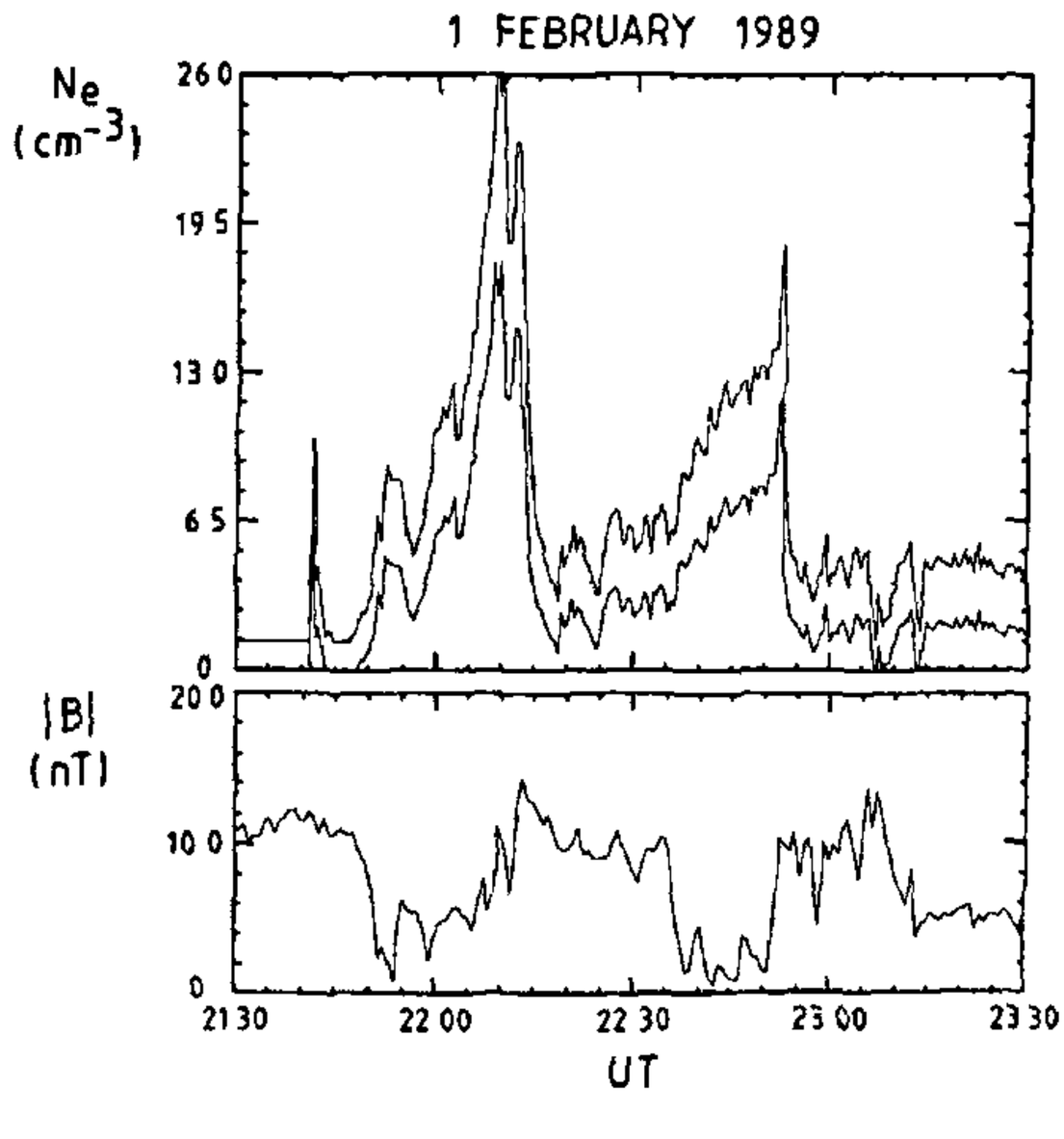

Figure 11. Electron density enhancements anticorrelated with magnetic field fluctuations in the tail planetosphere (8–10 Rms). The electron density is derived from spacecraft potential measurements; the upper and lower traces correspond to assumed mean kinetic energies of 1 and 8 eV, respectively[13].

Obstacle

The only available *in situ* ionospheric density and temperature data are those collected during the descents of the Viking landers, which are reproduced[23] in Figures 12 and 13.

The radio occultation measurements shown in Figures 14 and 15 confirm that peak densities of the order of 10^5 cm^{-3} are observed at altitudes around 125 km on the dayside[46, 47] and reveal that the ionosphere vanishes on the nightside[48].

Although the peak ionospheric thermal pressure is generally sufficient to stand off the solar wind[49], the existence of an overlying magnetic barrier extending up to an altitude of 500 km at the subsolar point, like at Venus[16] or a small intrinsic magnetic field, is required in order that the size of the obstacle be compatible with that of the observed shock[14].

The magnetization of the ionosphere of Venus by the solar wind has been observed experimentally but that of

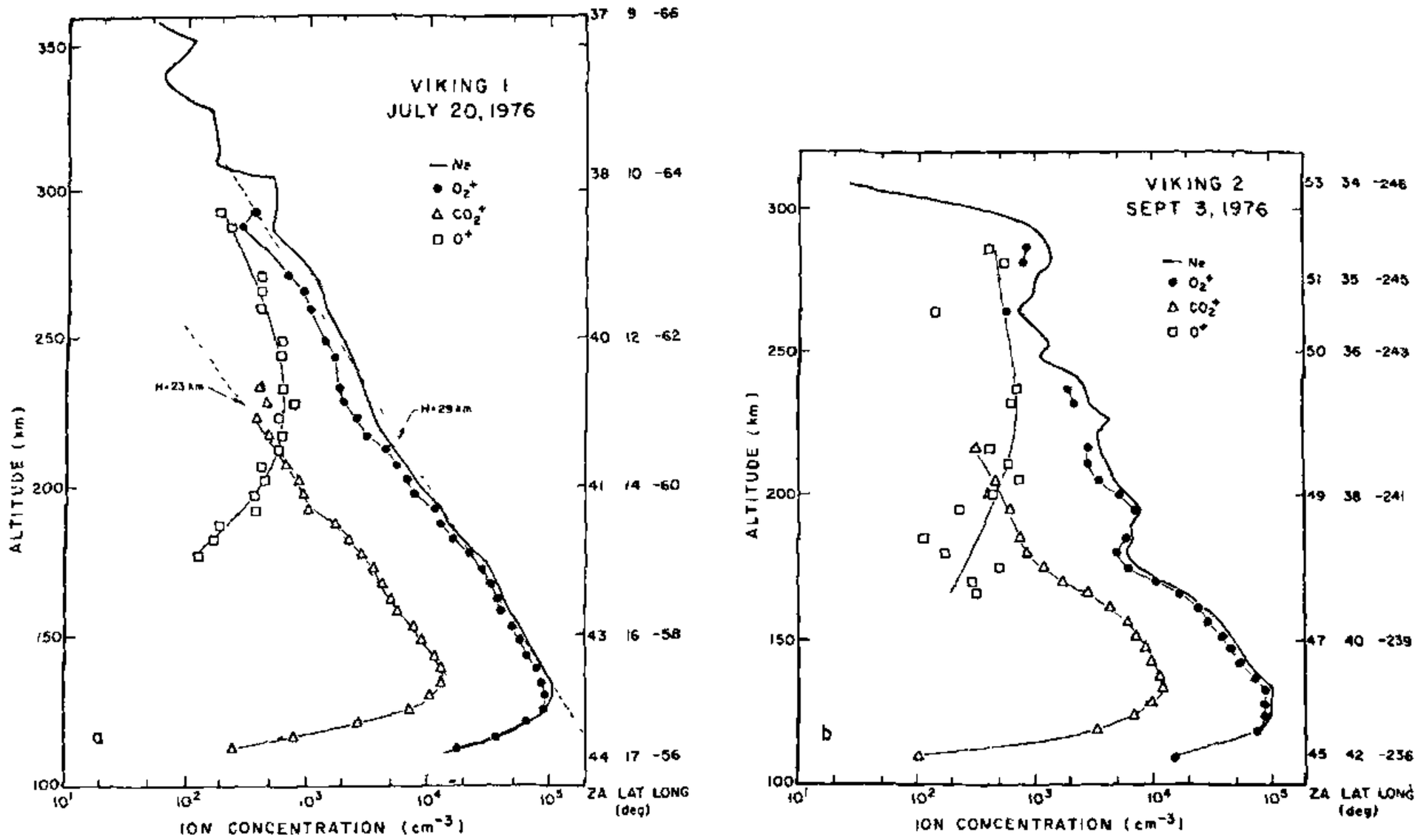

Figure 12. Individual and total ion concentrations observed during the descent of the Viking landers versus altitude and sublander Mars coordinates[23]

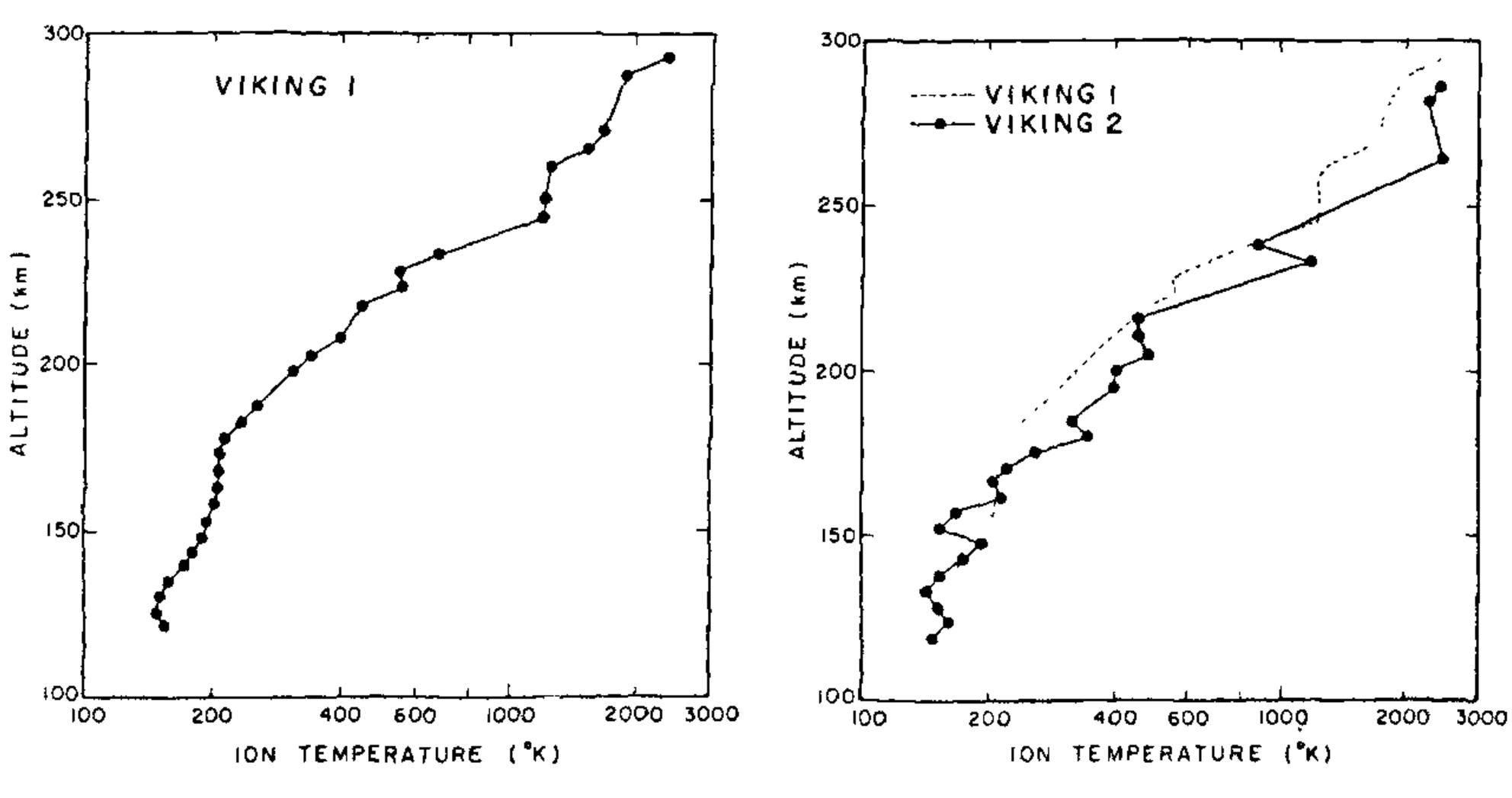

Figure 13. Ion temperature observed during the descent of the Viking landers[21]

Mars, although possible, remains so far unproven[16]. There is no consensus either about the possible existence of an intrinsic martian magnetic field[14, 50].

Tail

The tail of Mars is permeated by an induced magnetic field which results from the mass loading of the solar wind by planetary ions and the associated draping of interplanetary magnetic field lines[20]. The transition from the tail to the planetosphere is extremely smooth and the definition of the obstacle tail boundary is consequently somewhat academic (Figure 1).

The wave measurements collected by Phobos 2 at an aerocentric distance of 2.8 Rms are illustrated in Figure 6. The spacecraft crosses the tail during a time

interval of approximately 2 hours which covers the eclipse region corresponding to the middle section of each panel In eclipse, the broad-band and continuous electric noise level is reduced in the frequency range 0 3-3 kHz, presumably due to the absence of photoemission from the spacecraft and antenna surfaces and discrete bursts of waves and electron density enhancements are observed[51].

Figure 16 illustrates the diversity of phenomena which are recorded in the central part of the tail, during the traversal of the optical shadow of the planet. Cold electron clouds with densities of 10–100 cm^{-3} and mean kinetic energies of about 1 eV are encountered on nearly every orbit; these clouds are embedded in a much more tenuous ($\simeq 1$ cm^{-3}) and hotter (several 10 eV) electron environment. Comparing the electron and ion saturation currents collected by the Langmuir probe yields a much larger mean kinetic energy for the ions, of the order of several 100 eV. These plasma clouds differ from the density enhancement regions observed on the dayside (Figure 7, panel 2); the former are, in fact, observed in coincidence with the ion beams reported by Lundin *et al*[9] and Dubinin *et al.*[28]

These clouds are sometimes observed when the spacecraft crosses or approaches the neutral sheet, where the sign of B_x reverses (01.55 UT) The spectral extent of the wave emissions are often closely linked to the instantaneous level of the electron density (01:40-02:00 UT), but wave bursts are also observed when no significant increases of electron density are visible (02.00-02:30 UT).

It has been found at Venus that cloud formation was taking place near the terminator and was occurring in conjunction with orientation changes of the interplanetary field[52]; the existence of a similar process has not yet been established in the martian environment. It has also been proposed that planetary ions be removed by momentum transfer from the pickup ions to the upper ionospheric layers[43]. Parallel electric fields or magnetic field convection have been suggested as possible acceleration mechanism at Venus[53]; reconnection between intrinsic and captured magnetic field lines may also play a role at Mars[15]. The tailward ion outflow from Mars is estimated from Langmuir probe measurements to be in the ranges[51] $1.9–7.5 \times 10^{25}$ ions/s, in good agreement with independent O^+ flow measurements[9].

Conclusion

The wave activity in the upstream region of Mars is reminiscent of the emissions observed in the environment of other planets: electron plasma oscillations have been detected in the electron foreshock and instabilities developed by reflected or accelerated ions have been identified in the ion foreshock and shock foot The spectral signature of the shock region is in all aspects in agreement with that of all other planets.

The planetopause divides the downstream region which extends from the shock to the obstacle in two parts: the planetosheath and the planetosphere, respectively populated by a majority of solar wind protons and planetary ions. This boundary, which is easily identified and located with accuracy from plasma and wave observations at Mars, merges with the ionopause at Venus, except when the solar wind pressure is high, it is analogous with the cometopause observed near Halley[6].

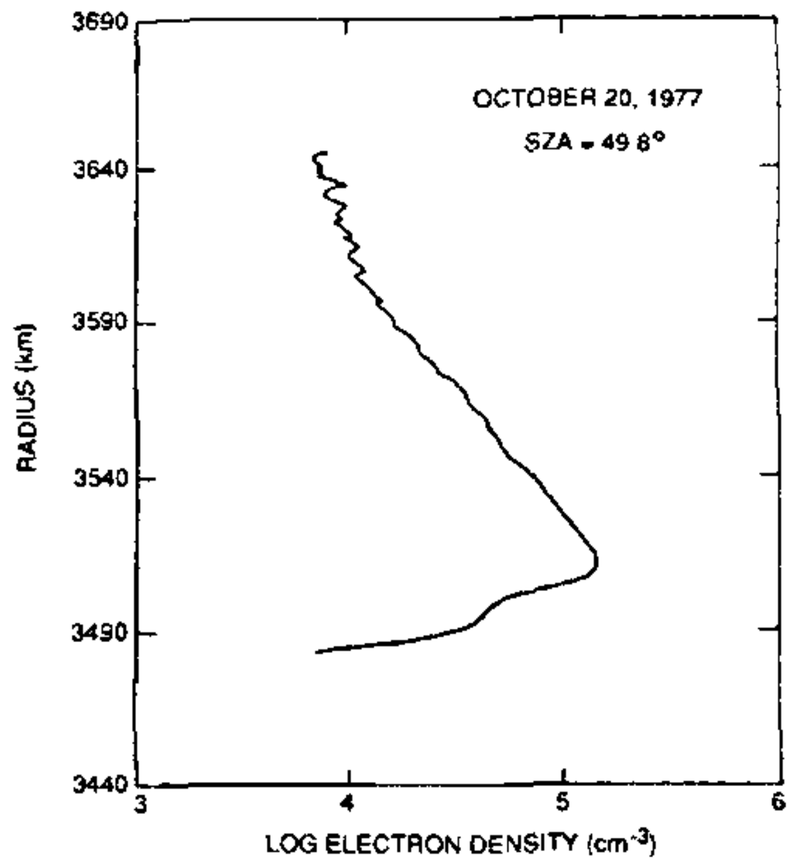

Figure 14. Day-time ionospheric electron density profile obtained with the Viking radio occultation experiment near solar minimum[46] Altitude = Radius – 3393 km

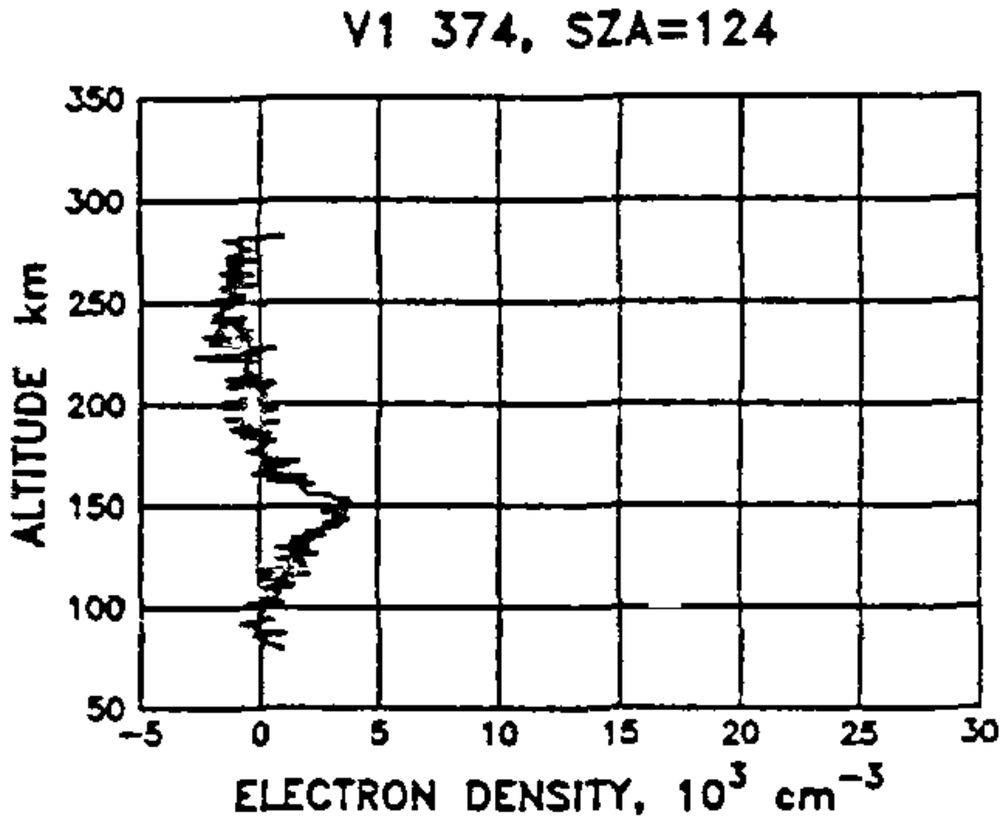

Figure 15. Night-time ionospheric electron density profile obtained with the Viking radio occultation experiment near solar minimum[48]

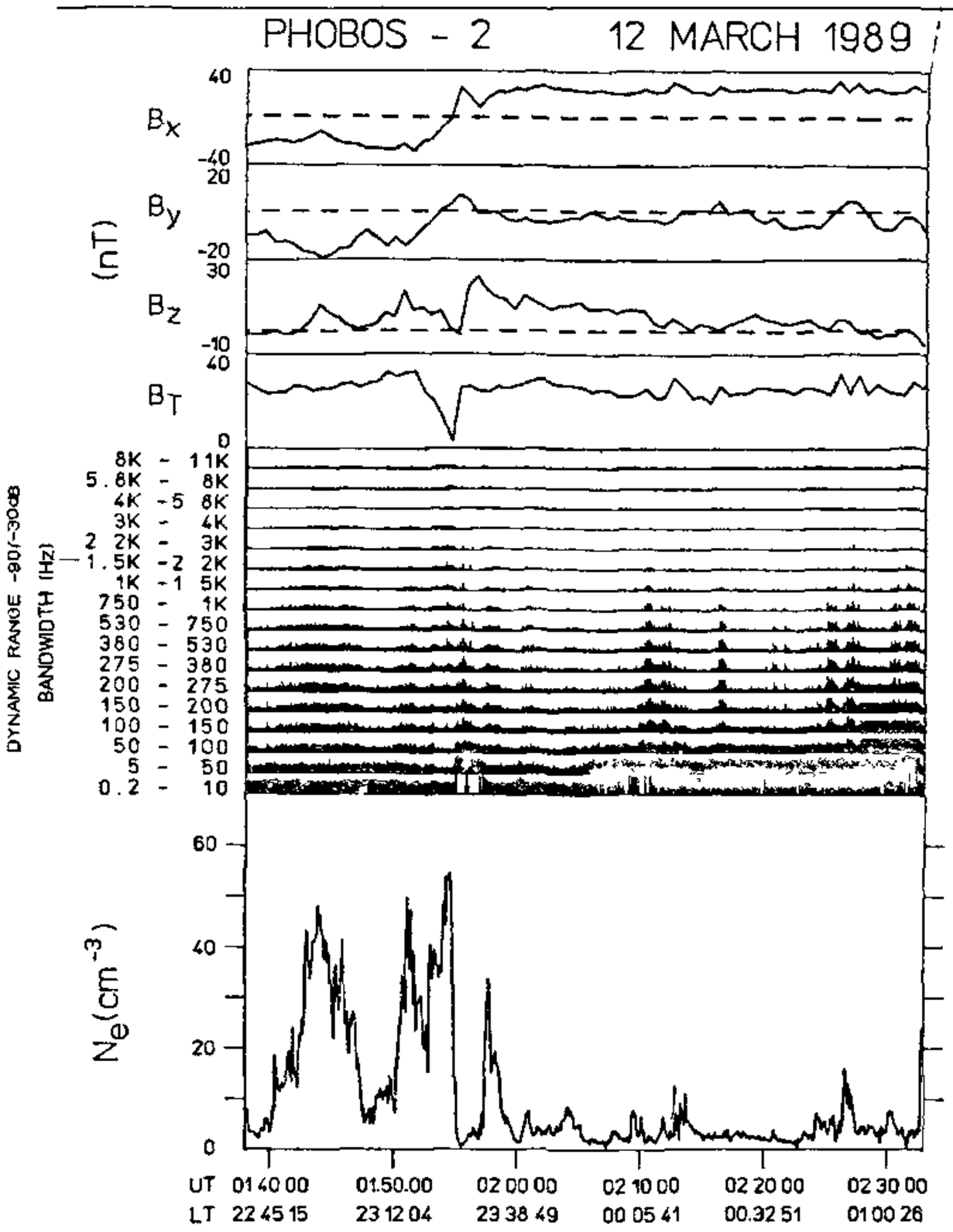

Figure 16. Plots of the magnetic field components and modulus, electric field signals and electron density versus universal time, local time and latitude at a distance of 2 8 Rms.The reference system is that of Figures 1 and 2 and latitude is measured with respect to the XY-plane.

The martian obstacle has not been clearly identified and its degree of magnetization is still problematic. Wave bursts and plasma clouds are permanent features of the martian tail and their relationship with magnetic structures is still under investigation.

The differences between the topologies of the Mars and Venus environments have been tentatively explained by the possibility that the former planet may possess an intrinsic magnetic field that would prevent the upward diffusion of ionospheric plasma[15].

It is expected that the forthcoming missions, Mars Observer and Mars 94, will answer these open questions.

1 Luhmann, J G , *Geophys Res Lett.*, 1990, **17**, 869–872
2 Moses, S L., Coronıti, F. V. and Scarf, F. L., *Geophys Res. Lett* , 1988, **15**, 429–432
3 Schwingenschuh, K , Riedler, W , Lichtenegger, H , Yeroshenko, Ye , Sauer, K , Luhmann, J G , Ong, M and Russell, C T , *Geophys Res Lett* , 1990, **17**, 889-892
4 Luhmann, J G and Brace, L H , *Rev Geophys* , 1991, **29**, 121-140
5 Grard, R , Narn, C , Pedersen, A , Klimov, S , Savin, S , Skalsky, A and Trotignon, J G , *Planet Space Sci* , 1991, **39**, 89-98
6 Breus, T. K., Krymskıi, A. M., Lundın, R , Dubinin, E M , Luhmann, J. G., Yeroshenko, Ye. G., Barabash, S V , Mıtnitskii, V. Ya., Passarenko, N. F. and Styashkın, V. A , *J Geophys. Res.*, 1991, **96**, 11165–11174.
7 Riedler, W. *et al.*, *Nature*, 1989, **341**, 604–607.
8. Grard, R., Pedersen, A., Klimov, S., Savin, S., Skalsky, A., Trotignon, J. G. and Kennel, C , *Nature*, 1989, **341**, 607–609.
9. Lundin, R., Zakharov, A , Pellinen, R., Borg, H., Hultqvist, B , Pissarenko, N , Dubinın, E. M., Barabash, S. W., Liede, I. and Koskinen, H., *Nature*, 1989, **341**, 609–612.
10 Rosenbauer, H. *et al* , *Nature*, 1989, **341**, 612–614
11. Shutte, N. M *et al.*, *Nature*, 1989, **341**, 614–616.
12. Lundın, R., Zakharov, A., Pellinen, R., Borg, H , Hultqvist, B , Pissarenko, N., Dubinın, E. M., Barabash, S. W., Liede, I and Koskinen, H., *Geophys. Res Lett* , 1990, **17**, 877–880.
13. Pedersen, A., Nairn, C., Grard, R. and Schwingenschuh, K.. *J. Geophys. Res* , 1991, **96**, 11243–11252.
14 Slavin, J. A., Schwingenschuh, K., Riedler, W. and Yeroshenko, Ye., *J. Geophys. Res.*, 1991, **96**, 11235–11241.
15. Axford, W. I , *Planet. Space Sci.*, 1991, **19**, 167–173.
16. Zhang, T. L., Luhmann, J G and Russell, C. T , *J Geophys. Res.*, 1991, **96**, 11145–11153
17. Johnson, F. S. and Hanson, W. B , *J. Geophys Res.*, 1991, **96**, 11097–11117.
18 Cravens, T. E and Shinagawa, H., *J. Geophys. Res* , 1991, **96**, 11119–11131.
19. Yeroshenko, Ye., Riedler, W., Schwingenschuh, K., Luhmann, J. G , Ong, M. and Russell, C. T., *Geophys. Res Lett* , 1990, **17**, 885–888.
20 Luhmann, J. G., Russell, C. T., Schwingenschuh, K. and Yeroshènko, Ye., *J. Geophys. Res.*, 1991, **96**, 11199–11208
21. Kliore, A., Cain, D. L., Levy, G. S., Eshleman, V. R , Fjeldbo, G. and Drake, F. D., *Science*, 1965, **149**, 1243–1248.
22. Fjeldbo, G., Sweetnam, D , Brenkle, J , Christensen, E., Farless, D., Metha, J., Seidel, B , Michael, Jr W., Wallio, A. and Grossi, M., *J. Geophys Res* , 1977, **82**, 4317–4324.
23 Hanson, W. B., Sanatini, S. and Zuccaro, D. R., *J. Geophys. Res* , 1977, **82**, 4351–4363.
24. Grard, R., Klinge, D., Klimov, S. and Trotignon, J. G., *J Phys E: Sci. Instrum.*, 1989, **22**, 888–894.
25. Sagdeev, R. Z. and Zakharov, A. V., *Nature*, 1989, **341**, 581–585.
26. Dubinin, E. M , Lundın, R., Pissarenko, N. F., Barabash, S V , Zacharov, A. V., Koskinen, H., Schwingenschuh, K. and Yeroshenko, Ye G., *Geophys. Res Lett* , 1990, **17**, 861–864
27. Horányi, M., Tóralfyay, M., Juhász, A and Luhmann, J G , *J. Geophys. Res.*, 1991, **96**, 11283–11290.
28. Dubinin, E. M., Pissarenko, N. F., Barabash, S. V , Zacharov, A V., Lundın, R., Pellinen, R., Schwingenschuh, K and Yeroshenko, Ye G., *Planet. Space Sci* , 1991, **39**, 113–121
29 Russell, C. T., Luhmann, J G , Schwingenschuh, K , Riedler, W and Yeroshenko, Ye., *Geophys Res Lett* , 1990, **17**, 897–900
30. Bogdanov, A. V , *J. Geophys Res* , 1981, **86**, 6926–6932
31. Dubinin, E. M., Pissarenko, N F , Barabash, S V , Zacharov, A. V., Lundın, R , Koskinen, H , Schwingenschuh, K and Yeroshenko, Ye. G , *Planet Space Sci* , 1991, **39**, 113–121
32 Skalsky, A , Grard, R , Klimov, S , Narn, C M C , Trotignon, J G. and Schwingenschuh, K , *J Geophys* , 1992, **97**, 2927–2933.
33 Tcheto, J and Faucheux, M , *J Geophys Res* , 1981, **89**, 6631 6653.
34. Crawford, G K , Strangeway, R W and Russell, C T , *Geophys Res Lett* , 1990, **17**, 1805–1808
35 Gurnett, D A , *Geophysical Monograph 35*, American Geophysical Union, 1985, pp 207 224
36 Sagdeev, R Z , Shapiro, V D , Shevchenko V I , Zachatov A , Kıraly, P , Szegö, K , Nagy, A F and Grard R J L , *Geophys Res Lett* , 1990, **17**, 893 896
37 Trotignon, J G , Grard R and Klimov, S , *Geophys Res Lett* 1991, **18**, 365–368

38 Sauer, K., Roatsch, Th., Motschmann, U., Möhlmann, D., Schwingenschuh, K. and Riedler, W., *Ann Geophys.*, 1990, **8**, 661–670
39 Moses, S. L., Kennel, C. F., Strangeway, R. J., Grard, R. and Nairn, C., *J Geophys Res.*, 1991, **96**, 11221–11226
40 Trotignon, J. G., Hamelin, M., Grard, R., Pedersen, A., Klimov, S., Savin, S., Skalsky, A. and Kennel, C., *Planet Space Sci.*, 1991, **39**, 99–112
41 Trotignon, J. G., Grard, R. and Savin, S., *J Geophys Res.*, 1991, **96**, 11253–11264
42 Scarf, F. L., Gurnett, D. A. and Kurth, W. S., *Nature*, 1981, **292**, 747–750
43 Perez-de-Tejada, H., *J Geophys. Res.*, 1991, **96**, 11115–11163
44 Riedler, W., Schwingenschuh, K., Lichtenegger, H., Möhlmann, D., Rustenbach, J., Yeroshenko, Ye., Achache, J., Slavin, J., Luhmann, J. G. and Russell, C. T., *Planet Space Sci.*, 1991, **39**, 75–81
45 Szegö, K., Shapiro, V. I., Shevchenko, V. D., Sagdeev, R. Z., Kasprzak, W. T. and Nagy, A. F., *Geophys. Res Lett.*, 1991, **18**, 2305–2308
46 Woo, R. and Kliore, A. J., *J Geophys Res.*, 1991, **96**, 11073–11082
47 Zhang, M. H. G., Luhmann, J. G., Kliore, A. J. and Kim, J., *J Geophys. Res.*, 1990, **95**, 14829–14839
48 Zhang, M. H. G., Luhmann, J. G. and Kliore, A. J., *J Geophys. Res.*, 1990, **95**, 17095–17102
49 Zhang, M. H. G. and Luhmann, J. G., *J Geophys. Res.*, 1992, **97**, 1017–1025
50 Zhang, T. L., Schwingenschuh, K., Lichtenegger, H., Riedler, W., Russell, C. T. and Luhmann, J. G., *J Geophys Res.*, 1991, **96**, 11265–11269
51. Nairn, C. M. C., Grard, R., Skalsky, A. and Trotignon, J. G., *J Geophys Res.*, 1991, **96**, 11227–11233
52 Ong, M., Luhmann, J. G., Russell, C. T., Strangeway, R. J. and Brace, L. H., *J Geophys Res.*, 1991, **96**, 11133–11144
53 Kasprzak, W. T., Grebowsky, J. M., Niemann, H. B. and Brace, L. H., *J Geophys Res.*, 1991, **96**, 11175–11187